Electric moments and charge deformation in even rare-earth nuclei*

Alan H. Shaw and J. S. Greenberg
Wright Nuclear Structure Laboratory, Yale University, New Haven, Connecticut 06520
(Received 11 February 1974)

We present measurements of $E2$ and $E4$ transition matrix elements, and related β_2 and β_4 deformations, for eight even rare earth nuclei, by exploiting the effect of electric quadrupole and electric hexadecapole excitation on the multiple Coulomb excitation of states in their ground state bands. The Coulomb excitation probabilities for the 0^+, 2^+, and 4^+ states in the ground state bands of the even rare earth nuclei ^{152,154}Sm, ^{158,160}Gd, ^{164}Dy, ^{166,168}Er, and ^{174}Yb have been measured with ^{4}He projectiles at several incident energies below the respective Coulomb barriers by direct detection, at backward angles, of elastically and inelastically scattered particles. The direct detection of scattered ^{4}He particles was employed in order to eliminate the uncertainties involved in the detection of the deexcitation γ rays, and to facilitate the determination of $M(E2;0^+\rightarrow 2^+)$ to about the $\frac{1}{2}\%$ accuracy required to obtain a meaningful measurement of $M(E4;0^+\rightarrow 4^+)$. Coulomb-nuclear interference effects in elastic and inelastic scattering were investigated, and it was demonstrated that Coulomb nuclear interference occurs at a much lower projectile energy than predicted by the simple classical formula for the Coulomb barrier, and manifests itself at different incident energies for elastic and inelastic scattering. The data on excitation probabilities were analyzed both with a semiclassical Coulomb excitation calculation, corrected for quantal effects in second order perturbation theory, and with a full quantal calculation, to determine the reduced electric transition matrix elements $M(E2;0^+\rightarrow 2^+)$ and $M(E4;0^+\rightarrow 4^+)$. Significant differences were found between the perturbation theory quantal treatment and the full quantal calculations. Static quadrupole and hexadecapole moments of the charge distribution were extracted from the measured transition matrix elements within the context of the rotational model. Using an axially symmetric deformed Fermi shape to parametrize the charge distribution, charge deformation parameters β_2^C and β_4^C, deduced from the static moments, were found to follow the same general trends as the potential deformation parameters measured in nuclear scattering experiments well above the Coulomb barrier. For some nuclei the Coulomb excitation β_λ^C values show what may be significant deviations from the nuclear potential deformations parameters. However, it is emphasized that, presently, the significance of such a comparison as well as the significance of a comparison with deformation parameters determined with other electromagnetic probes, is subject to the considerations introduced by the model dependence of each measurement, and diluted by the ambiguous correspondence between the quantities being measured in the different experiments.

[NUCLEAR REACTIONS ^{152,154}Sm(α,α'), ^{158,160}Gd(α,α'), ^{164}Dy(α,α'), ^{166,168}Er(α,α'), ^{174}Yb(α,α'), $E_\alpha = 8$–17 MeV; measured Coulomb excitation probabilities. Deduced $B(E2)$, $B(E4)$; extracted β_2, β_4 from rotational model and Fermi charge distribution. Enriched targets.]

1. INTRODUCTION

Information on nuclear size, the shapes of nuclei, and the distribution of nucleons in the nucleus has provided a continuing important stimulus to the development of theories of nuclear structure, and also served as a gauge of their success. With the accumulation of extensive and precise measurements of quadrupole deformations in nuclei, recent studies have focussed on the higher moments of both the charge and nuclear interaction potential distributions. There is presently considerable theoretical interest in the magnitude of the higher moments, since it is anticipated that higher multipole components of the nuclear matter distribution can influence nuclear properties in important ways. For example, some recent calculations, which include a hexadecapole component in the potential for single particle motion, have demonstrated that the equilibrium shapes are sensitive to the presence of even a small hexadecapole component.[1-3]

Experimental evidence for the existence of hexadecapole and higher multipole components in the shapes of nuclei has been accumulating from measurements employing both strong interaction and electromagnetic interaction probes. Typical of the former studies are investigations of elastic and inelastic scattering of strongly interacting projectiles with energies well above the Coulomb barrier,

where nuclear scattering dominates.[4-7] The deformation parameters derived from these measurements are most directly associated with the deformed nuclear potential field distribution used to describe the nuclear scattering.[4-7] Through complex calculations they possibly can be related to the mass and charge distributions. Nuclear scattering experiments at lower projectile energies have utilized Coulomb-nuclear interference to extract charge deformation information.[8] However, the analysis of such data cannot avoid whatever ambiguities are involved in the modeling of the nuclear interaction via a deformed optical potential. More direct information on the charge distribution can be obtained by exploiting measurements involving purely electromagnetic interaction mechanisms such as hyperfine interactions in atoms, electron scattering, and Coulomb excitation, although it must be recognized that the interpretation of these measurements in terms of a spatial parametrization of the charge distribution and the comparison of information from the three experimental techniques depends on adopting models for the nuclear shape and nuclear dynamics. Comparing shape parameters derived from the nuclear and the electromagnetic probes requires a further understanding of the detailed relationship between the nuclear potential distribution and the charge distribution, since the two types of measurements sample these different aspects of the nuclear shape.

Among the techniques involving electromagnetic interactions, in the past Coulomb excitation has been one of the more prolific sources of information on electric quadrupole matrix elements.[9] Recently Stephens *et al.*[10] demonstrated the feasibility of employing Coulomb excitation with ^{4}He projectiles to extract electric hexadecapole transition moments and their related charge deformation parameters, β_4^C, in deformed nuclei. Other Coulomb excitation investigations of hexadecapole deformations in rare earth nuclei have since been reported by Saylor *et al.*,[11] Erb *et al.*,[12] Ebert *et al.*,[13] Brüchner *et al.*,[8] and Greenberg and Shaw.[14] The β_4^C values deduced from these measurements closely follow the trends exhibited by the potential deformation parameters, β_4^N, obtained from nuclear scattering experiments.[4,5] Except for the possible exceptions of ^{152}Sm and ^{154}Sm, the magnitudes of β_4 values obtained from experiments below and above the Coulomb barrier are also substantially similar for most of these nuclei, although the large uncertainty associated with a Coulomb excitation measurement of a small positive or negative β_4 value[15] renders these comparisons only qualitative for many of the cases studied. Because of the latter limitations, the measurements for ^{152}Sm and ^{154}Sm become particularly interesting and meaningful examples since their large positive β_4 values, among the largest positive values encountered in rare earth nuclei, may allow quantitative comparisons to be made with nuclear potential scattering experiments. Both nuclei have been investigated extensively with Coulomb excitation[8,10-14] and inelastic electron scattering.[16] Although there are some disagreements among these measurements, which in part depend on the analysis procedures and nuclear shape parameters adopted, two of the measurements[10,14] indicate that the charge and mass distributions may be significantly different in both ^{152}Sm and ^{154}Sm, as reflected in a factor of 2 difference between β_4 values obtained from these experiments and nuclear scattering probes.[4-7] Similar differences also have been observed by Bemis *et al.*[17] in their comprehensive Coulomb excitation investigations of even-A actinide nuclei.

We have extended our precision Coulomb excitation studies with ^{4}He projectiles[14] and in this report we summarize all our measurements of $E2$ and $E4$ transition moments and their related β_2^C and β_4^C deformations for the ground state members of eight even rare earth nuclei, ^{152,154}Sm, ^{158,160}Gd, ^{164}Dy, ^{166,168}Er, and ^{174}Yb. For all cases the direct detection of elastically and inelastically scattered particles was employed in order to attain the accuracy required to obtain a meaningful measurement of $M(E4; 0^+ \rightarrow 4^+)$. The experimental arrangement was similar to the one adopted by Berant *et al.*[18] in their precision Coulomb excitation measurements with ^{4}He projectiles. Coulomb-nuclear interference effects both in inelastic and elastic scattering were investigated. The data were analyzed with a full quantal Coulomb excitation calculation.

General consideration of the experimental method, the choice of experimental parameters, and details on the experimental method are presented in Sec. 2. Section 3 deals with the data processing method which yields the Coulomb excitation probabilities for the 0^+, 2^+, and 4^+ states of the ground state band. These excitation probabilities are analyzed for the following quantities in a sequence which utilizes an increasing number of model assumptions: (1) the reduced transition matrix elements $M(E2; 0^+ \rightarrow 2^+)$ and $M(E4; 0^+ \rightarrow 4^+)$, which are extracted most directly from the excitation probabilities using Coulomb excitation calculations; (2) the static quadrupole and hexadecapole moments of the charge distribution, deduced from the transition matrix elements and assumptions based on the rotational model; (3) the charge deformation parameters β_2^C and β_4^C, derived from the static moments assuming a deformed Fermi shape for the charge distribution. Details of this analysis and

important considerations associated with the Coulomb excitation technique are discussed in Secs. 4 and 5. A comparison of the present data with deformation parameters obtained by other methods, and the current significance of a such a comparison, are outlined in Secs. 5C and 6.

2. EXPERIMENTAL METHOD

A. General considerations

Although an accurate calculation of the $E4$ matrix element contribution to the Coulomb excitation process can only be approached by solving a complete set of coupled equations for the excitation amplitudes, some insight can be gained, and a fairly accurate estimate can be made of the effect, by examining the simplified case of a target nucleus with only 0^+, 2^+, and 4^+ states excited by incident ^{4}He projectiles. Only first and second order processes are considered. This is a reasonable approximation to the situation encountered in this experiment, since the excitation of all other states is almost negligible.

Using the formulation of Alder, Roesel, and Morf,[19] the probability of exciting the 4^+ state of the ground state rotational band by direct $E4$ and double $E2$ excitations can be written, in second order perturbation theory,

$$P(4)=P_{0\to2\to4}^{(2,2)}\left[1+\frac{\chi_{0\to4}^{(4)}}{\chi_{0\to2}^{(2)}\chi_{2\to4}^{(2)}}\,d(\xi_1,\xi_2,\eta,\theta)+\left(\frac{\chi_{0\to4}^{(4)}}{\chi_{0\to2}^{(2)}\chi_{2\to4}^{(2)}}\right)^2 a(\xi_1,\xi_2,\eta,\theta)\right], \quad (2.1)$$

where

$$P_{0\to2\to4}^{(2,2)}=(\chi_{0\to2}^{(2)})^2(\chi_{2\to4}^{(2)})^2\Pi_4(\xi_1,\xi_2,\eta,\theta) \quad (2.2)$$

is the excitation probability due to $E2$-$E2$ excitation, and where $\chi_{I_0\to I}^{(\lambda)}$ and a are given by

$$\chi_{I_0\to I}^{(\lambda)}=\frac{\sqrt{16\pi}(\lambda-1)!}{(2\lambda+1)!!}\,\frac{Z_1 e}{\hbar(v_{I_0}v_I)^{1/2}}\,\frac{\langle I_0\|\mathfrak{M}(E\lambda)\|I\rangle}{a^{\lambda}(2I_0+1)^{1/2}},$$

$$a=\frac{Z_1Z_2e^2}{mv_0v_1}. \quad (2.3)$$

(2.4)

The notation is from Alder *et al.*[19] where the functions $d(\xi_1,\xi_2,\eta,\theta)$, $a(\xi_1,\xi_2,\eta,\theta)$, and $\Pi_4(\xi_1,\xi_2,\eta,\theta)$ are tabulated. The excitation probability $P(4)$ can thus be written as

$$P(4)=P_{0\to2\to4}^{(2,2)}\left[1+C(\xi_1,\xi_2,\eta,\theta)\frac{Q_4}{Q_2^2}+C'(\xi_1,\xi_2,\eta,\theta)\left(\frac{Q_4}{Q_2^2}\right)^2\right], \quad (2.5)$$

where the functions C and C' depend [illegible]

matics and contain the functions $d(\xi_1,\xi_2,\eta,\theta)$ and $a(\xi_1,\xi_2,\eta,\theta)$, respectively, as multiplicative factors. The quantities Q_4 and Q_2 are the intrinsic hexadecapole and quadrupole moments calculated from the reduced matrix elements by the rotational model prescription

$$M(E\lambda;I_i\to I_f)=\langle I_i\|\mathfrak{M}(E\lambda)\|I_f\rangle=(2I_i+1)^{1/2}\langle I_i0\lambda0\,|\,I_f0\rangle Q_\lambda. \quad (2.6)$$

The behavior of the functions C and C' with η are shown in Fig. 1, as is the variation of the total $E4$ contribution to the excitation probability of the 4^+ state for a typical case. In the range of useful bombarding energies below the Coulomb barrier (8 to 12 MeV), the variation of the $E4$ contribution with projectile energy is slight. The dependence on scattering angle is illustrated in Fig. 2. In that part of the lanthanide rare earths where the rotational model is known to give an accurate description of the low-lying states of even-even nuclei, Q_2

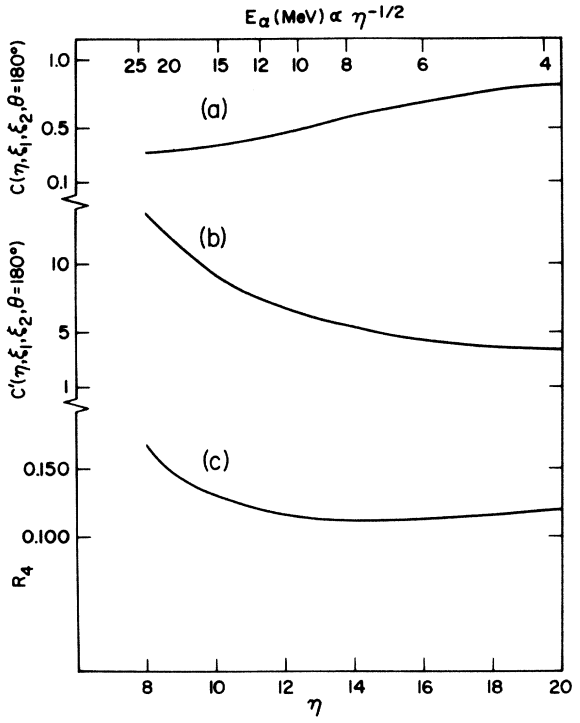

FIG. 1. Dependence on the Sommerfeld parameter, η, of (a) the function $C(\eta,\xi_1,\xi_2,\theta=180°)$, (b) the function $C'(\eta,\xi_1,\xi_2,\theta=180°)$, and (c) $R_4=[P(4)]/(P_{0\to2\to4}^{(2,2)})-1$, the total $E4$ contribution to $P(4)$ for $Q_4/Q_2^2=0.1$ as described in Eq. (2.5) for a typical even rare earth rotational nucleus; $E_{2+}=0.080$ MeV, $E_{4+}=0.260$ MeV, $\xi_1=0.262\times10^{-5}\eta^3$, $\xi_2=2.25\,\xi_1$. It should be noted that for incident energy below 8 MeV, $P(4)$ is too small to facilitate a reasonable Coulomb excitation measurement, while above 12 MeV the scattering is no longer pure

varies little with mass number, and the magnitude of the $E4$ contribution to $P(4)$ is dictated solely by Q_4.

Although these estimates are reasonably valid in the situation usually encountered with light projectiles, they are not generally applicable in the case of heavy projectiles, since multiple processes proceeding through many other states can effect the excitation of the 4^+ state as much as the direct $E4$ excitation. The general problem is thus best examined in terms of a full coupled channels Coulomb excitation calculation[9] for various projectiles exciting a given target under conditions of specified beam energy and scattering angle. We briefly summarize a few results of such calculations which are pertinent to this work. A more general discussion can be found in a paper by Winkler.[15]

Figure 3 represents the results of semiclassical coupled channels calculations[9] performed for back angle scattering with incident energies close to the Coulomb barrier. It shows the variation with incident projectile charge of the $E4$ contribution to the excitation probability of states in the ground state band of a nucleus such as ^{154}Sm. For a given state, the magnitude of this contribution decreases with increasing Z_p; but for a given projectile it increases with the spin of the state being studied. Since the excitation probability, in general, decreases with increasing state spin for a given projectile, it is not always possible, in practice, to take advantage of the increase in the magnitude of the $E4$ contribution with state spin by observing states higher up in the band. A contribution of 20 to 30% is about the largest that can be conveniently observed for a nucleus such as ^{154}Sm under realistic experimental conditions; measuring the larger ratios R_I predicted for the higher spin states would necessitate prohibitively long data accumulation times.

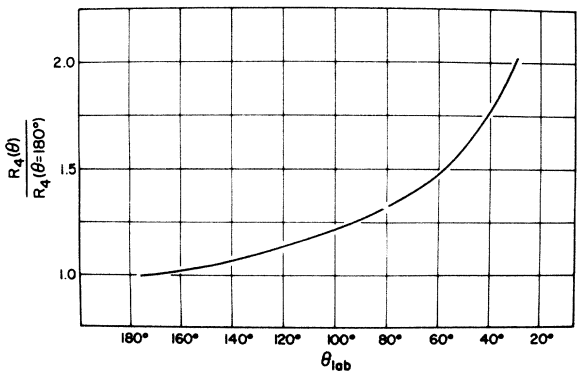

FIG. 2. Variation with scattering angle of the $E4$ contribution to $P(4)$ for ^{4}He excitation of a typical rotational nucleus; $\eta = 12$, $\xi_1 = 0.045$, $\xi_2 = 0.101$.

In principle, by taking advantage of the variation of the $E4$ contribution and multiple $E2$ excitation with bombarding species, with state spin, and with incident energy, it should be possible to judiciously select experimental situations in which each contributing matrix element is uniquely determined from a measured excitation probability. Thus, in principle, it is possible to construct the entire transition matrix for the ground state band. For example, if low energy ^{4}He projectiles are employed, the excitation of the 2^+ state depends only on $M(E2; 0^+ \rightarrow 2^+)$, since the $E4$ contribution is very small and the multiple excitation of the 4^+ state from the 2^+ is negligible at low enough bombarding energies. Using low energy ^{16}O beams to excite the 4^+ state, $P(4)$ depends predominantly on the product $M(E2; 0^+ \rightarrow 2^+) \times M(E2; 2^+ \rightarrow 4^+)$; with $M(E2; 0^+ \rightarrow 2^+)$ determined to high accuracy from the previous measurement, the $M(E2; 2^+ \rightarrow 4^+)$ matrix element is uniquely determined from $P(4)$. The additional use of ^{4}He or Li projectiles at incident energies close to the Coulomb barrier to excite the 4^+ state by double $E2$ and competing direct $E4$, leads to the extraction of $M(E4; 0^+ \rightarrow 4^+)$ as the only additional unknown.

This procedure can be followed with heavier projectiles to include higher excited states. However, multiple $E2$ and multiple $E4$ excitation becomes increasingly important to the excitation of states with spin greater than 4; therefore, in practice, the situation becomes complicated for the higher spin states, necessitating some assumptions and independent measurements of interband transitions which begin to make significant contributions.[20-22]

Herein we concentrate on the determination of

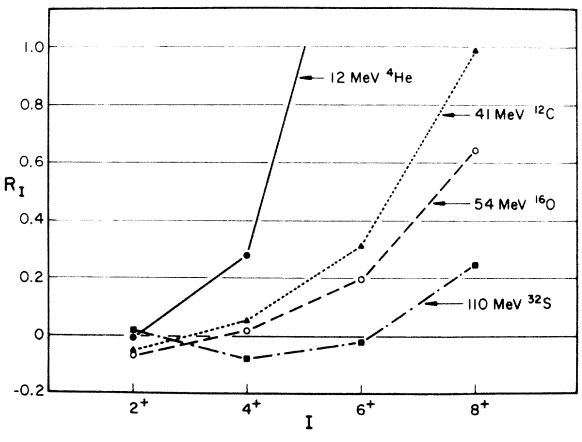

FIG. 3. The $E4$ contribution to the excitation of states in the ground state band of a typical rare earth nucleus with $M(E2; 0^+ \rightarrow 2^+) = -2.066\, e\,\text{b}$, $M(E4; 0^+ \rightarrow 4^+) = 0.653\, e\,\text{b}^2$, which is a reasonable approximation to ^{154}Sm; $\theta_{lab} = 175°$, $R_I = (P_{(1)}^{(E2,E4)} - P_{(1)}^{(E2)})/P_{(1)}^{(E2)}$. The incident energies indicated are close to the Coulomb barrier.

the matrix elements $M(E2; 0^+ \rightarrow 2^+)$ and $M(E4; 0^+ \rightarrow 4^+)$. These matrix elements are extracted in the most straightforward manner, i.e. with the least dependence on a knowledge of other matrix elements, and on assumptions involving the validity of the rotational model for states with spin greater than 4. As the above discussion indicates, ^{4}He projectiles are particularly useful for determining these matrix elements. The measurements of $P(2)$ and $P(4)$ with ^{4}He projectiles yields $M(E2; 0^+ \rightarrow 2^+)$ directly, and $M(E4; 0^+ \rightarrow 4^+)$ with only the additional determination of $M(E2; 2^+ \rightarrow 4^+)$. As was pointed out above, the $E4$ contribution to $P(4)$ with this choice of projectile is as large as the effect expected in any other experimental configuration. The present report is confined to measurements with ^{4}He projectiles only, and the results rely on other sources for the matrix element $M(E2; 2^+ \rightarrow 4^+)$.

The technical advantage of using ^{4}He projectiles lies in that it is possible to sufficiently resolve the inelastically scattered α particles from the elastic scattering peak to extract the excitation probabilities to a high degree of accuracy, while avoiding the uncertainties involved in detecting deexcitation γ rays.[10,13] The direct detection of the inelastically scattered projectiles provides a straightforward normalization and avoids the necessity for accurate calibration of absolute and relative counting efficiencies that would be inherent in a measurement in which the deexcitation γ rays are detected. In addition, the calculation of the excitation probabilities from γ ray spectra requires an accurate determination of internal conversion coefficients especially for the low energy γ radiations from the $(2^+ \rightarrow 0^+)$ transition.

A backscattering geometry was chosen for the present measurements. The detection of the incident particles scattered at back angles into an annular detector centered on the incident beam axis offers several advantages, besides the obvious one of symmetry. (a) The excitation probabilities are maximized near 180°, while the Rutherford cross section is smallest, and varies most slowly with angle there. (b) The kinematic spread in the peaks is minimized at back angles, allowing a large solid angle without undue loss in energy resolution. The large solid angle is dictated by the high statistical accuracy required for these measurements. [The detectors employed spanned a polar angle of approximately 3°, which corresponds to roughly a change of $\frac{1}{2}$% in $P(2)$ and $P(4)$ across the face of the detector, or $\pm\frac{1}{4}$% about the central angle, the variation being roughly linear with angle.] (c) The kinematic separation of the contaminant lines is maximized at back angles, so that the elastic lines from possible light element contaminants not present in the isotope sample—such as zirconium from the target preparation process and copper from the electrodes of the evaporation equipment—would, if present, be well separated from the lines of interest.

The contributions from contaminants in the samples from which the targets are fabricated are a major problem with a scattering experiment of this type. High purity samples are required. Another problem is resolution loss due to the projectiles losing energy in the target, which dictates the use of very thin targets. These thin targets must be supported on carbon backings, introducing pileup problems due to the large count rate originating from the $^{12}C(\alpha, \alpha')^{12}C$ and $^{16}O(\alpha, \alpha')^{16}O$ reactions. These problems are dealt with in more detail below.

The magnitude of the uncertainties in determining $M(E4; 0^+ \rightarrow 4^+)$ from such measurements can be estimated by noting that in the most favorable cases it is expected that the $E4$ contribution to $P(4)$ is approximately 25–30%, whereas the smallest contributions are expected to be 10% and less. The uncertainty in determining the contribution from $E4$ excitation varies from four times to possibly ten times the percentage uncertainty in the excitation probability of the 4^+ state. The extraction of the hexadecapole contribution to the excitation of the 4^+ state depends directly upon the accuracy with which the multiple $E2/E2$ contribution can be correctly calculated. An uncertainty in $M(E2; 0^+ \rightarrow 2^+)$ of $\frac{1}{2}$% results in an uncertainty in the calculated $P(4)$ of about $1\frac{1}{2}$% and an uncertainty in the extraction of the $E4$ contribution of 5 to 15%, assuming the uncertainty in $M(E2; 2^+ \rightarrow 4^+)$ to be the same as that in $M(E2; 0^+ \rightarrow 2^+)$. The best measurements of $M(E2; 2^+ \rightarrow 4^+)$ claim an accuracy of $1\frac{1}{2}$ to 2%,[23] and these measurements exist only for the samarium isotopes. If the rotational model is used to calculate that matrix element from $M(E2; 0^+ \rightarrow 2^+)$, its uncertainty must reflect not only the uncertainty in $M(E2; 0^+ \rightarrow 2^+)$, but also the degree to which the model is applied to correctly predict it[17]; this will be treated at greater length in a subsequent section. The uncertainty in the calculation of $P(4)$ is therefore expected to be roughly 3%, assuming the uncertainty in $M(E2; 0^+ \rightarrow 2^+)$ to be small compared to the uncertainty in $M(E2; 2^+ \rightarrow 4^+)$. It was therefore decided to attempt to measure $P(4)$ to 2–3% accuracy and $P(2)$ to 1% accuracy [which yields $M(E2; 0^+ \rightarrow 2^+)$ to about $\frac{1}{2}$% accuracy].

B. Experimental arrangement

The experiment was performed using ^{4}He beams from the Yale University MP1 tandem Van de

Graaff accelerator. The beam energy calibration was checked by comparing the energy of elastically scattered projectiles to a calibration determined using a ^{212}Pb α particle emitting source. The deviation was found to be only 5 to 10 keV from the nominal value. The beams had short term stabilities of $\pm\frac{1}{4}$ keV and a long term stability better than 1 keV.

The scattering geometry is shown in Fig. 4. The accuracy of these measurements depends critically on achieving good energy resolution and large peak to valley ratios. Slit scattering therefore was carefully investigated and steps were taken to minimize it. The beam was passed through three polished tantalum collimators separated by approximately 10 cm, the last of which was mounted on the back of the detector mount. The target, 4.5 cm from the detector, was surrounded by a cryogenic trap. Thin polished Lucite collimators were employed to define the active area of the detector and other baffles were arranged to minimize secondary scattering into the detector. The mean scattering angle of the detector was approximately 175°.

The detector was operated below room temperature to reduce leakage current and noise, thus improving resolution. The shape and relative height of the low energy tail of the peaks were studied as a function of detector bias; the detector bias was progressively increased until the tail ceased to show improvement. The detectors were run at large overbias.

The resolution, full width at half maximum (FWHM), for 8.78 MeV α particles from a ^{212}Pb source, was 13 to 14 keV. Spectra obtained for elastic scattering from the thinnest targets, which produced typical count rates of 5–10/sec, resulted in a broadening of the system resolution, as measured with the source, by less than 1 keV. The ratios achieved for the 2^+ inelastic peak height to the valley between the 2^+ peak and the elastic peak for thin ^{152}Sm targets were as good as 80:1, while,

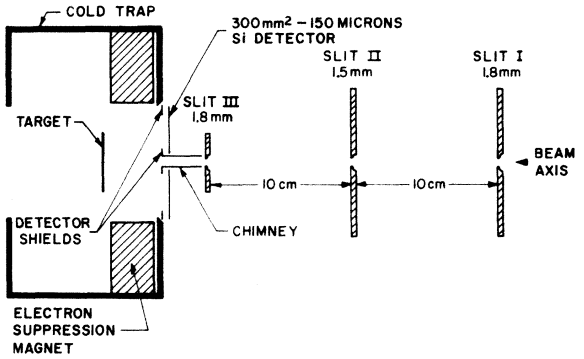

FIG. 4. Scattering geometry.

for those rare earth targets with lower 2^+ state energies, the peak to valley ratios were about 25:1. The elastic peak to background ratios were 20 000:1 to 30 000:1. These thinnest targets were used to measure $P(2)$. To obtain reasonable counting statistics in the 4^+ inelastic peak, it was necessary to increase the count rate by employing thicker targets, which broadened resolution by about 3 keV and produced peak to valley ratios of 17:1–20:1 for the 2^+ states. Peak to valley ratios for ^{152}Sm were considerably greater. The accompanying decrease in resolution did not present a problem, due to the greater separation of the 4^+ state.

The thin rare earth targets were fabricated from oxide samples obtained from the stable isotope separation facility at Oak Ridge National Laboratory. Most of the samples were better than 98.5% enriched, and several purities exceeded 99.9%. With the exception of the gadolinium isotopes, all the samples were reduced with zirconium and simultaneously evaporated by resistance heating in a carbon boat. The gadolinium samples were obtained in metallic form and evaporated using electron bombardment heating. In all cases the samples were evaporated directly onto commercially available 10 μg/cm^2 carbon foils. Some targets were prepared with a thin layer of ^{208}Pb deposited prior to the deposition of the rare earth, providing a normalization for elastic scattering and a convenient monitor of the peak shape.

Under normal experimental conditions, count rates for α particles scattered from the rare earth target material averaged from 5/sec to 50/sec. However, the total count rate on occasion was as large as 10^4/sec, originating principally from elastic and inelastic scattering from the carbon backing material. The pulse height distribution of the latter pulses was sufficiently separated from the primary data as to constitute a pulse pileup problem only. The use of a pileup rejection system made it possible to use incident beam currents of up to 350 nA without observing the characteristic high energy peak broadening due to pulse pileup. Target degeneration problems, however, dictated a limit in beam intensity of 200–250 nA.

3. RESULTS: EXPERIMENTAL EXCITATION PROBABILITIES

Thick and thin target spectra for ^{152}Sm are shown in Fig. 5; spectra for ^{160}Gd, which are more representative of the other nuclei studied, are shown in Fig. 6. For each target nucleus the excitation probabilities $P(2)$ and $P(4)$ were measured at several incident energies below the effective Coulomb barrier. The working definition of the Coulomb

barrier was derived from additional studies which explored the deviation from pure Coulomb elastic and inelastic scattering as a function of the projectile energy for both ^{152}Sm and ^{154}Sm, using the elastic scattering from ^{208}Pb for normalization and a composite ^{208}Pb-Sm target. The projectile energy region investigated in the latter measurements was 8–17 MeV. The use of these data to determine the "safe" bombarding energy is discussed in more detail in Sec. 4 C.

A thick ^{154}Sm spectrum before and after the subtraction of background and known target contaminants is shown in Fig. 7. The backgrounds were mostly flat, varying from 1–2 counts per channel for thin target spectra to 8–9 counts per channel for some of the thick target spectra. The peaks due to known contaminants listed in the assays of the isotope samples were subtracted using the shape of the elastic peak.

Two related methods were employed to unfold the spectra into their constituent spectral lines. In both cases the criteria were the same: the three peaks were required to have the same shape, and the low energy tail on each peak was constrained to be a smooth function similar in shape to the tail of an isolated ^{208}Pb elastic peak. In one of the methods employed, an iterative manual fitting procedure was followed in which the first approximation to the shape of the elastic peak tail was the tail of a well defined ^{208}Pb peak.

In the second method, a computer fitting routine was used to fit all three peaks simultaneously using

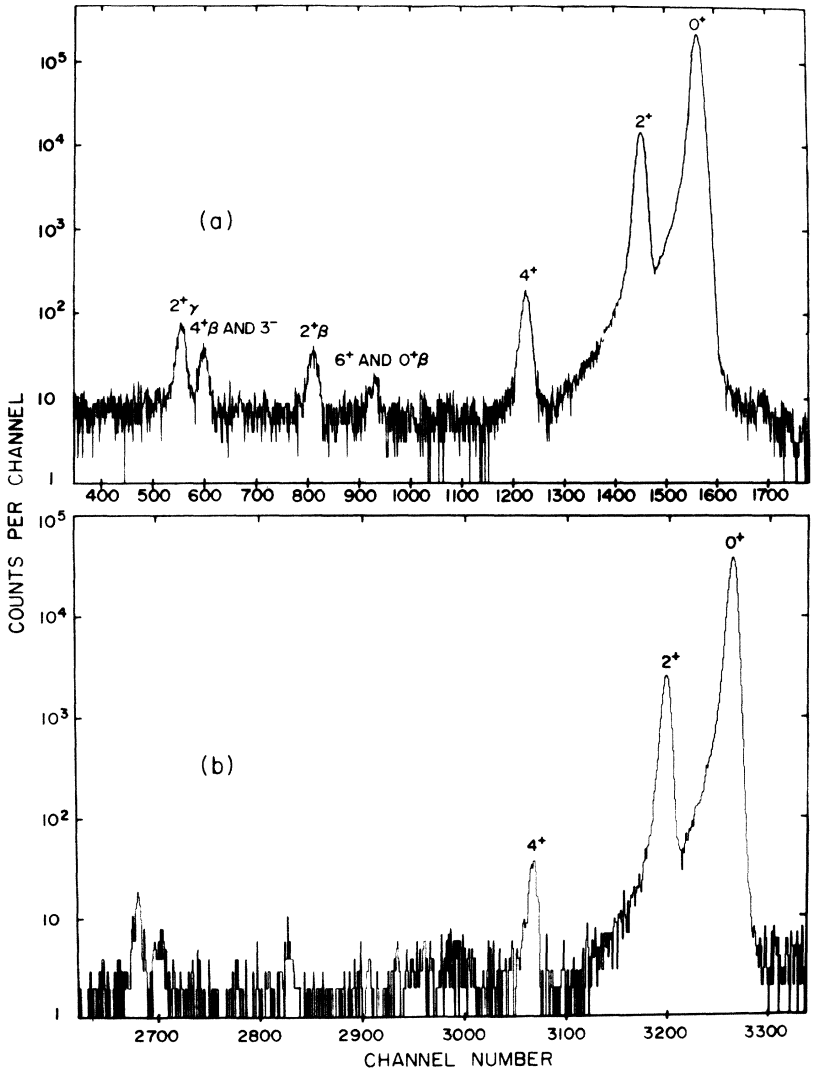

FIG. 5. Spectra of ^{4}He scattered from ^{152}Sm targets: (a) 11.75 MeV ^{4}He scattered from a thick target at $\theta_{lab}=174.5°$; (b) 12.00 MeV ^{4}He scattered from a thin target at $\theta_{lab}=174.5°$.

the elastic peak shape and a tail which is a hyperbola on a semilogarithmic representation of the spectral shape. The tail was appended to the empirical peak shape at a point which was not a variable of the fit, so that the function had the form:

$$f(x) = A_1 \exp\{[(x - A_3)^2 A_4^4 + A_5^2]^{1/2} + (x - A_3)A_2^2\}$$

for $x \leq x'$

$$= \text{SPECT}(x) \quad \text{for } x > x' , \tag{3.1}$$

where SPECT(x) is the measured number of counts at channel x. The form chosen for the inelastic peaks was

$$g_N(x) = c_N f(x - x_N), \tag{3.2}$$

so that they differed from the elastic peak only in their relative normalization c_N, and relative position x_N. The starting parameters for the tail were the result of a fit to a ^{208}Pb peak. The uncertainties determined by the computer fit, calculated by comparing the final shapes of the peaks, were equivalent to those obtained using the manual fitting procedure. Typical uncertainties in the determination of $P(2)$ and $P(4)$ were 1–2% and 2–4%, respectively, including statistical errors. These excitation probabilities are defined here as:

$$P(2) = d\sigma_{\text{lab}}(2^+)/[d\sigma_{\text{lab}}(0^+) + d\sigma_{\text{lab}}(2^+) + d\sigma_{\text{lab}}(4^+)],$$
$$P(4) = d\sigma_{\text{lab}}(4^+)/[d\sigma_{\text{lab}}(0^+) + d\sigma_{\text{lab}}(2^+) + d\sigma_{\text{lab}}(4^+)]. \tag{3.3}$$

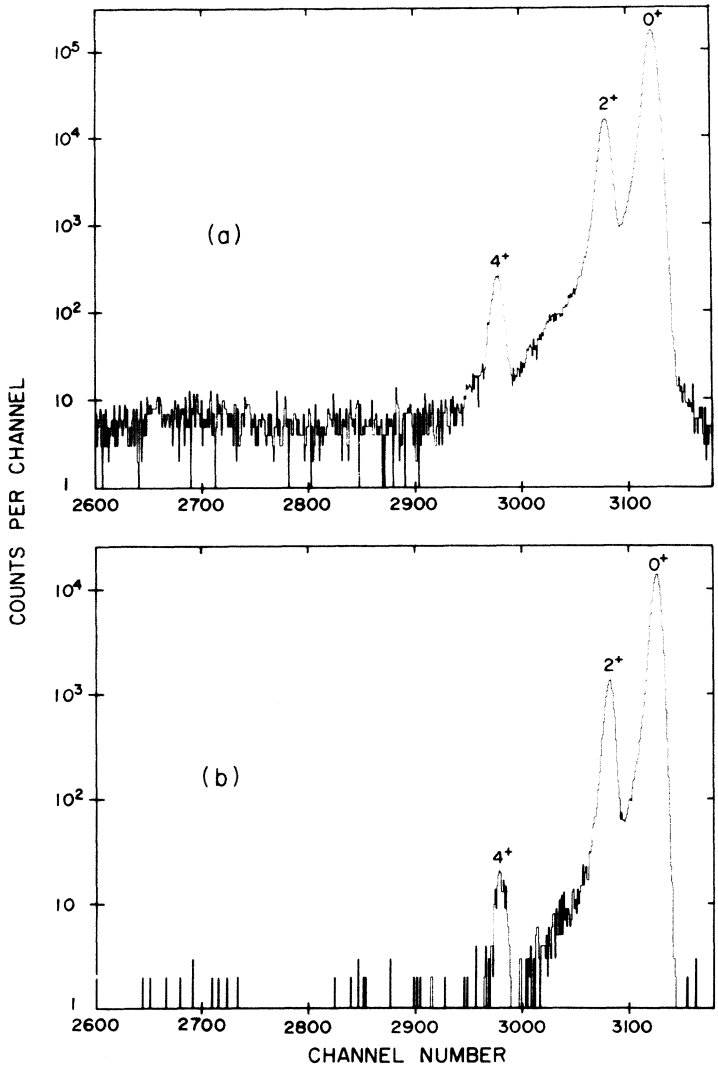

FIG. 6. Spectra of ^{4}He scattered from ^{160}Gd targets. These spectra are typical of the nuclei ^{154}Sm to ^{174}Yb, which all have similar energy level spacings. (a) 11.75 MeV ^{4}He scattered from a thick target at $\theta_{\text{lab}} = 174.5°$. (b) 11.75 MeV ^{4}He scattered from a thin target at $\theta_{\text{lab}} = 174.5°$.

The measured excitation probabilities are tabulated in Table I.

4. ANALYSIS

A. Calculation of excitation probabilities

The calculations of the excitation probabilities from the reduced matrix elements were carried out in part using a version of the deBoer-Winther semiclassical multiple Coulomb excitation code[9] which includes $E1$, $E2$, $E3$, and $E4$ transitions. It has been pointed out[24] that for the conditions encountered in this experiment, where the Sommerfeld parameter $\eta = 10-15$, quantal effects are not negligible for multiple excitations. The semiclassically calculated excitation probabilities therefore were corrected for quantal effects, in one procedure that was followed, using the second order perturbation calculation by Alder *et al.*[19] We note that the quantal corrections modify the excitation probability of the 2^+ state by direct $E2$ and double $E2$ via the reorientation effect by roughly 2%, and the excitation probability of the 4^+ state due to double $E2$ and competing direct $E4$ by about 6%. Exploratory calculations of the full quantal formulation of this scattering problem were carried out using the code LISA.[25] The results of that calculation differ somewhat from the perturbation treatment. This point is discussed in detail in Sec. 4 D.

Calculations of the excitation probabilities using the deBoer-Winther code included states up to 8^+ in the ground state rotational band, as well as the 2^+_γ vibrational state, the 0^+ and 2^+ members of the β vibrational band, and the 1^- and 3^- states, where these states have been identified. The reduced

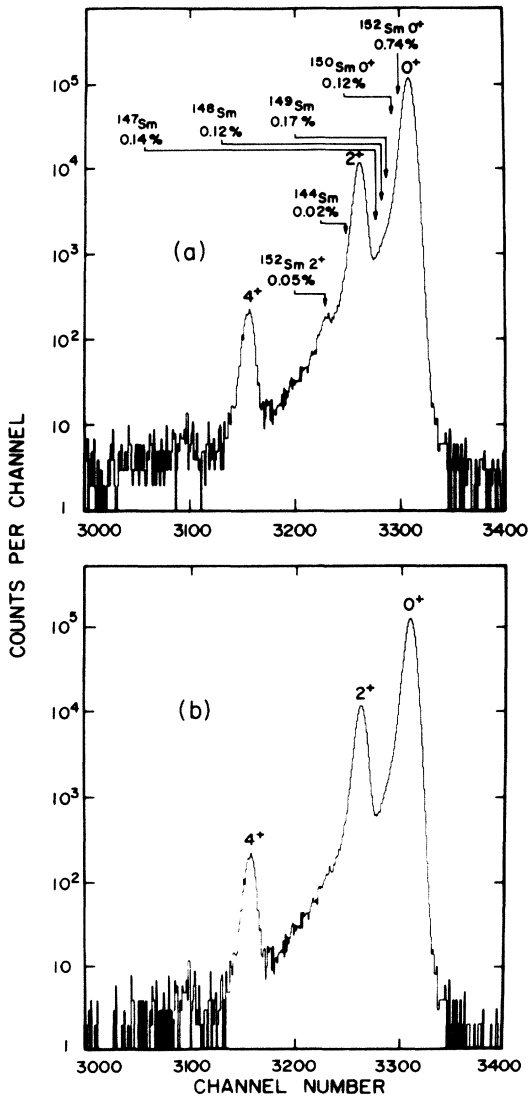

FIG. 7. ^{154}Sm$(\alpha, \alpha')^{154}$Sm spectrum before (a) and after (b) subtraction of background and known contaminants. $E_\alpha = 12.25$ MeV $\theta_{lab} = 171.5°$.

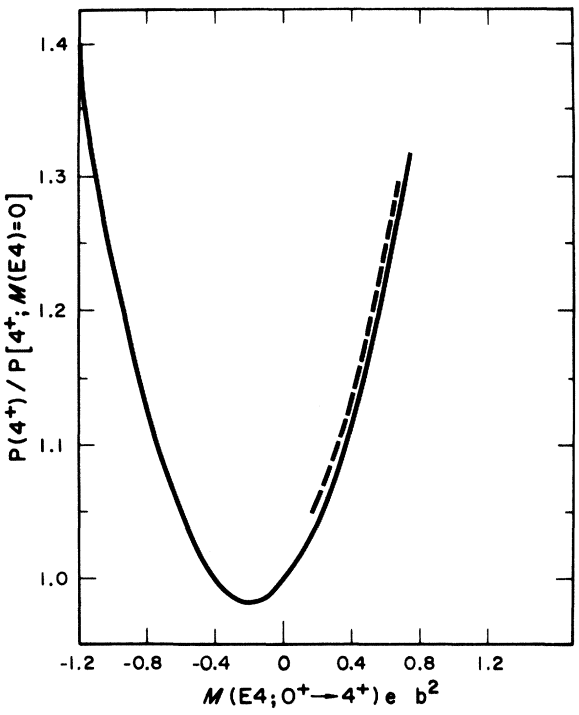

FIG. 8. The variation of the $E4$ contribution to $P(4)$ with $M(E4; 0^+ \rightarrow 4^+)$ for ^{4}He excitation of ^{154}Sm. All $E4$ matrix elements are related to $M(E4; 0^+ \rightarrow 4^+)$ through the rotational model. $E_\alpha = 12$ MeV, $\theta_{lab} = 175°$. Quantal corrections are included. There are two values of $M(E4; 0^+ \rightarrow 4^+)$ for each possible $P(4)$. The figure also demonstrates the error introduced by using only a three level (0^+, 2^+, 4^+) calculation (dashed line) rather than the full 11 level calculation (solid line).

TABLE I. Experimentally measured excitation probabilities for ^{4}He excitation, and ratios of total scattering from ^{152}Sm and ^{154}Sm to scattering from ^{208}Pb. The samarium to lead ratios are normalized to the average from 8–12 MeV incident energy, and the statistical standard deviations on these ratios are $\frac{1}{2}\%$ for ^{152}Sm and $\frac{3}{4}\%$ for ^{154}Sm. See text for definition of the excitation probabilities. The percent standard deviations in the excitation probabilities are shown in parentheses. An asterisk indicates a laboratory scattering angle of 171.5°; otherwise it is 174.5°.

	^{152}Sm			^{154}Sm		
E_{inc} (MeV)	Sm/Pb	$P(2)$	$P(4)$	Sm/Pb	$P(2)$	$P(4)$
8	1.006	0.0188(2.8)*		0.988		
9	0.992	0.0269(2.6)*		1.005		
9.5	1.005			1.005		
10	1.001	0.0374(2)*		1.014		
		0.0376(2.2)				
10.5	0.997	0.0438(2)*		1.004		
10.75	0.996					
11	1.001	0.0500(2)*		0.995	0.0641(1.3)	
		0.0507(1)				
		0.0501(1.7)				
11.25	1.001				0.0705(1.5)	
11.5	1.002	0.0570(2)*	0.000 634(3.5)	1.003	0.0754(1.7)	0.001 06(3)*
		0.0578(1.5)				
11.75	1.004		0.000 724(2)	0.997	0.0783(1.3)*	0.001 23(3)
12	0.996	0.0639(1)		0.988	0.0832(1.3)	0.001 47(3)
		0.0641(1)				
		0.0649(2)*	0.000 833(2)			
		0.0649(1.5)	0.000 829(2)			
12.25	1.005	0.0676(1.4)		1.014	0.0867(1.2)*	0.001 62(3)*
					0.0887(2.5)	
12.5	0.998	0.0719(2)*		1.008	0.0937(2.2)	0.001 75(2.2)*
		0.0743(2)				
12.75	1.003	0.0767(2)		0.995	0.0950(3)	
13	0.991	0.0805(1.2)	0.001 34(2)	0.989	0.0994(1.3)	0.002 31(3)
		0.0792(1.5)				
		0.0786(2)				
		0.0793(2)*				
13.25	0.982	0.0852(2)*		1.002		
		0.0845(1.8)				
13.5	0.988	0.0893(2)*		0.989		
		0.0892(2)				
13.75	0.982	0.0900(2)*		0.984		
14	0.959	0.0954(2)*		0.970		
		0.0957(2.5)				
14.25		0.1005(2)*		0.975		
14.5	0.939	0.1065(2)*		0.929		
14.75				0.918		
15	0.901	0.1120(2)*				
		0.1128(1.5)				
15.25				0.848		
15.5		0.1252(2)*				
15.75				0.782		
16	0.742	0.1405(2)*				
		0.1412(1.8)				
16.5				0.621		
17	0.559					

TABLE I *(Continued)*

E_{inc} (MeV)		^{158}Gd	^{160}Gd	^{164}Dy	^{166}Er	^{168}Er	^{174}Yb
11.00	$P(2)$					0.0623(1.7)	0.0563(1.5)
	$P(4)$						
11.25	$P(2)$						
	$P(4)$						
11.50	$P(2)$	0.0748(1.2)*	0.0780(1.3)				0.0638(1.5)
							0.0639(1.5)
	$P(4)$						0.000 623(3.5)
11.75	$P(2)$	0.0805*(1.3)	0.0846(1.3)	0.0801(2)			
			0.0852(1.3)	0.0798(1)			
	$P(4)$	0.001 21(2.7)	0.001 29(2.6)	0.001 30		0.000 992*(3)	0.000 773*(3.5)
12.00	$P(2)$	0.0842*(1.3)	0.0892(1.3)	0.0846(1.5)*	0.0785(1.5)	0.0809(1.5)	0.0732(1.8)
				0.0846(1)*		0.0805(1.5)	
	$P(4)$		0.001 43(3)	0.001 15(3)*	0.001 09(4)	0.001 15(2.5)	0.000 913(3.5)
12.25	$P(2)$	0.0893*(1.2)	0.0937(1.3)		0.0823*(1.3)		
	$P(4)$	0.001 54*(3)	0.001 66(3)		0.001 22*(3)	0.001 29*(3)	
12.50	$P(2)$						
	$P(4)$						
12.75	$P(2)$						
	$P(4)$						
13.00	$P(2)$				0.0975(1.3)		0.0915(1.3)
	$P(4)$				0.001 81(3)		0.001 53(3.5)

matrix elements used in the calculation are listed in Table II. Those not listed were calculated from $M(E\lambda; 0 \rightarrow \lambda)$ using the rotational model. The effect of excluding all states except the 0^+, 2^+, and 4^+ states in a calculation of $P(4)$ is shown in Fig. 8 for ^{154}Sm.

The sensitivity of the calculation of $P(2)$ and $P(4)$ to variations in the matrix elements used in the calculation is shown in Table III. The sensitivity of $P(2)$ to all matrix elements other than $M(E2; 0^+ \rightarrow 2^+)$ is clearly negligible compared to the accuracy with which that excitation probability is experimentally determined. The effect of experimental uncertainties in the matrix elements to higher states is inconsequential since they have been determined to a higher degree of accuracy than the ±100% used in the calculation. The major error in the calculation of $P(4)$ derives from the uncertainties in $M(E2; 0^+ \rightarrow 2^+)$ and $M(E2; 2^+ \rightarrow 4^+)$. The latter is known from lifetime measurements for the samarium isotopes[23] with a standard deviation of about 1.8%. No such precision measurements exist for the other nuclei studied in this experiment, and the rotational model was therefore employed to calculate $M(E2; 2^+ \rightarrow 4^+)$ for those nuclei.

Some estimate of the error introduced by this assumption can be obtained by using some simple models to calculate the deviations from rotational model behavior. For example, it has been demonstrated that for both actinide[17] and lanthanide[22] nuclei, the centrifugal stretching model[26] overestimates the measured deviations from rotational behavior. In this model the transition matrix elements are calculated with the assumption that the deviations from rotational model values are totally reflected in the deviations due to centrifugal stretching effects in the energy level sequence from the simple rotational relationship

$$E = AI(I+1).$$

A calculation employing the rotational-vibrational interaction in a procedure which was used to successfully reproduce the prominent deviations from rotational behavior in $E2$ matrix elements observed in ^{152}Sm[22] indicates that the deviations from rotational values should not be significant in the cases of the nuclei ^{158}Gd to ^{174}Yb. In fact, if this centrifugal stretching "worst case" analysis is applied to these nuclei, the maximum error introduced in the calculation of $P(4)$ by using the rotational value of $M(E2; 2^+ \rightarrow 4^+)$ is 1 to 2%. This error in combination with twice the error due to the uncertainty in $M(E2; 0^+ \rightarrow 2^+)$ results in a total error in the calculation of $P(4)$ of 2.5%. It should be noted that the excitation probability of the 6^+ state, the next most highly populated state in the ground state band, is roughly 2 orders of magnitude less than $P(4)$, and the error introduced by using the rotational model value for higher transition matrix elements is therefore negligible.

The variation of $P(4)$ with $M(E4; 0^+ \rightarrow 4^+)$, as illustrated in Fig. 8, was obtained by using rotational model values based on $M(E4; 0^+ \rightarrow 4^+)$ for all other $E4$ matrix elements. There are, in general, two possible values of $M(E4; 0^+ \rightarrow 4^+)$ which fit the

data: a positive solution and a negative one. The positive solution is always taken here, since, even in the case of ^{174}Yb where β_4 is expected to be most negative, the negative solution for $M(E4; 0^+ \rightarrow 4^+)$ results in an unreasonably large negative β_4. This will be dealt with in greater detail in Sec. 5 B.

The values of $M(E2; 0^+ \rightarrow 2^+)$ and $M(E4; 0^+ \rightarrow 4^+)$ from these measurements, after all corrections are made, are tabulated in Table IV and the trend vs A is illustrated in Fig. 9. The errors include the uncertainties in the individual determinations, the spread in the individual values about the weighted average, and the calculational uncertainties discussed above.

TABLE II. Matrix elements used in the analysis in units of $e\,b^{\lambda/2}$. Those not listed were calculated from the rotational model.

Nucleus	λ	J^π_i	J^π_f	$M(E\lambda; J_i \rightarrow J_f)$	Reference
^{152}Sm	2	2^+	4^+	−2.98	a
	2	4^+	6^+	−3.93	b
	2	6^+	8^+	−4.79	b
	2	0^+	$2^+\beta$	−0.151	b
	2	2^+	$2^+\beta$	0.360	b
	2	4^+	$2^+\beta$	−0.675	b
	2	2^+	$0^+\beta$	−0.425	b
	2	2^+	$4^+\beta$	−0.22	b
	2	4^+	$4^+\beta$	0.58	b
	2	0^+	$2^+\gamma$	−0.30	b
	2	2^+	$2^+\gamma$	−0.48	b
	2	4^+	$2^+\gamma$	−0.15	b
	2	2^+	$4^+\gamma$	−0.20	b
	2	4^+	$4^+\gamma$	−0.64	b
	1	0^+	1^-	0.017	b
	1	2^+	3^-	−0.024	b
	3	0^+	3^-	−0.43	b
^{154}Sm	2	2^+	4^+	−3.267	a
	2	0^+	$2^+\beta$	−0.141	c
	2	0^+	$2^+\gamma$	−0.263	c
	3	0^+	3^-	−0.277	c
	3	0^+	3^-	−0.232	c
^{158}Gd	2	0^+	$2^+\gamma$	−0.3	d
^{160}Gd	2	0^+	$2^+\gamma$	−0.3	e
^{164}Dy	2	0^+	$2^+\gamma$	−0.35	f
^{166}Er	2	0^+	$2^+\gamma$	−0.4	g
^{168}Er	2	0^+	$2^+\gamma$	−0.4	g

[a] Reference 23.
[b] J. S. Greenberg, I. A. Fraser, and R. Stokstad, private communication.
[c] Reference 10.
[d] O. Nathan and V. I. Popov, Nucl. Phys. 21, 631 (1960); quoted in Nucl. Data A5 (No. 6), 115 (1964).
[e] B. Elbek, B. Herskind, N. C. Olesen, and Y. Yoshizawa, Nucl. Data A5 (No. 6), 132 (1964).
[f] T. Grotdal, K. Nybø, T. Thorsteinson, and B. Elbek, Nucl. Phys. A110, 385 (1968).
[g] J. M. Domingos, G. D. Symons, and A. C. Doublas, Oxford University Report No. 21/71 (unpublished).

B. Further corrections

In obtaining the matrix elements and their uncertainties listed in Table IV, several other effects not previously mentioned were taken into account. (1) Vacuum polarization and atomic screening of the nuclear electric potential were considered. Since both these corrections are small, they are adequately treated by considering only their effect on the orbit of the projectile. Saladin, Glenn, and Pryor[27] present an expression for the effect of atomic screening on the electric potential energy at separation distances short compared to the atomic radius. In this treatment, the center-of-mass bombarding energy used in the deBoer-Winther code is altered by the calculated change in potential energy. Foldy and Eriksen[28] present a similar expression for the change in potential energy due to vacuum polarization. Treating both in a similar manner, the former results in an increase in the effective bombarding energy of 20–30 keV, while the latter produced a decrease of the effective center-of-mass bombarding energy that is somewhat larger. The net result is compensated for by lowering the effective bombarding energy by about 15 keV. This results in a change in the

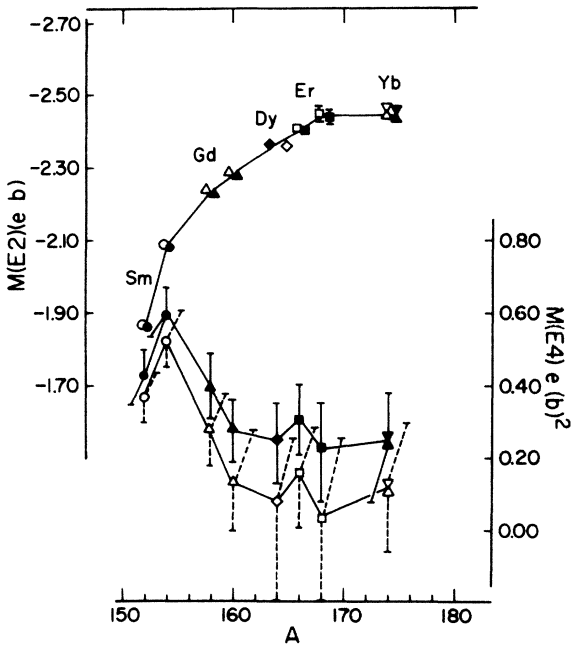

FIG. 9. Measured $M(E2; 0^+ \rightarrow 2^+)$ and $M(E4; 0^+ \rightarrow 4^+)$ as a function of mass number. The open symbols indicate Set I obtained using second order perturbation theory and the closed symbols indicate Set II obtained with the code LISA.

$M(E2; 0^+ \rightarrow 2^+)$ value of 0.18% and a similarly small change in the $M(E4; 0^+ \rightarrow 4^+)$ value.
(2) The difference between the beam energy as determined using the ^{212}Pb source and the nominal energy results in a change roughly half of that due to the combination of vacuum polarization and screening effects. The excitation probabilities of the 2^+ and 4^+ states change by 0.3% and 0.6%, respectively, from the central angle to either extreme angle admitted by the detector. This variation is roughly linear across the face of the detector, and results in an uncertainty of about 0.1% in $M(E2; 0^+ \rightarrow 2^+)$ and about 0.2% in $M(E4; 0^+ \rightarrow 4^+)$, when the cross sections are calculated at the central angle rather than integrated across the detector face. The uncertainty in the measurement of the central angle results in a 0.02% uncertainty for the 2^+ excitation probability.

C. Nuclear interference effects

The primary studies to determine the Coulomb barrier were conducted for elastic scattering and inelastic scattering to the 2^+ state of ^{152}Sm. These were complemented by similar studies of ^{154}Sm which were conducted to search for any possible difference between the results for a transitional nucleus such as ^{152}Sm and the more statically deformed nuclei beginning at ^{154}Sm. Although using the classical expression for the Coulomb barrier, which assumes the target and projectile just "touch," is grossly in error in this case, it is probably correct to assume that for nuclei of similar structure the barrier energy scales according to the classical form—i.e., as the ratio of nuclear charges.

The ratio of scattering from samarium to scattering from ^{208}Pb is shown for both isotopes in Fig. 10. The values of $M(E2; 0^+ \rightarrow 2^+)$ extracted as a function of energy under the assumption of pure Coulomb excitation are shown in Fig. 11. Although Fig. 10 shows no significant deviations from pure Coulomb scattering below about 13 MeV, the inelastic data displays deviations on the 1% level beginning at about 12 MeV. This is consistent with similar data obtained by Bruckner *et al.*[8] on ^{152}Sm; these authors also studied scattering from the 4^+ state as a function of bombarding energy. Using an optical potential plus Coulomb scattering they were able to fit their data successfully through approximately the range of incident energies shown here, from the region of pure Coulomb scattering to the region of dominant nuclear scattering. In addition, their calculation predicts that deviations in the 4^+ state occur at about the same energy as deviations in elastic scattering in the mass 150 region. This prediction fits their data. No systematic deviation in $M(E4; 0^+ \rightarrow 4^+)$ was observed up to 13 MeV in this experiment. The ^{154}Sm data reveals similar effects, with measureable non-Coulomb effects beginning at somewhat higher incident energies. Only data obtained at incident energies of 12 MeV or less were used to determine the quadrupole and hexadecapole transition moments of the samarium isotopes, while the highest incident energies used in the analysis of the gadolinium, dysprosium, and heavier targets were 12.25, 12.5, and 13 MeV, respectively. Recent studies by Stelson *et al.*[29] of both $P(2)$ and $P(4)$ as a function of incident ^{4}He energy for ^{154}Sm, ^{166}Er, and ^{182}W support this determination of the "safe" bombarding energies.

D. Full quantal calculation

The computer code LISA [25] solves the set of coupled equations of the partial wave expansion of the

TABLE III. The effects of changes in the matrix elements used in the calculation of the excitation of a typical even rare earth nucleus by incident ^{4}He projectiles. These do not necessarily represent experimental uncertainties in the matrix elements, especially in the case of interband transitions.

Matrix elements(s) changed	$M(E2; 0^+ \rightarrow 2^+)$ (%)	$M(E2; 2^+ \rightarrow 4^+)$ (%)	All $E4$ matrix elements within ground state band (%)	All $E2$ matrix elements to γ band (%)	All $E2$ matrix elements to β band (%)	All matrix elements to 1^-, 3^- states (%)
Change	1	2	20	100	100	100
Effect on calculated $P(2)$	2	0.06	0.002	0.22	0.2	0.1
Effect on calculated $P(4)$	2	4	4	0.5	0.3	0.01

TABLE IV. Experimentally determined matrix elements $M(E2;0^+ \rightarrow 2^+)$ and $M(E4;0^+ \rightarrow 4^+)$ in units of $e\,b^{\lambda/2}$, and the Coulomb deformation parameters β_2^C and β_4^C determined from them using the radial charge distribution parameters of Ref. 31 and a deformed Fermi charge distribution. Those values marked I, were determined from the analysis in which the semiclassical Coulomb excitation calculation was corrected for quantal effects using the perturbation calculation of Ref. 19. Those values marked II refer to the analysis with the quantal corrections derived from the LISA quantal calculations.

Nucleus	$M(E2;0^+ \rightarrow 2^+)$	$M(E2;0^+ \rightarrow 2^+)$ Other measurements	$M(E4;0^+ \rightarrow 4^+)$	$M(E4;0^+ \rightarrow 4^+)$ Other measurements	β_2^C	β_2^C Other measurements	β_4^C	β_4^C Other measurements
^{152}Sm	-1.865 ± 0.012 I	-1.844 ± 0.033 [a]	0.373 ± 0.070 I		0.287 ± 0.006 I	0.304 [a]	0.070 ± 0.020 I	
	-1.856 ± 0.012 II	-1.830 ± 0.020 [b]	0.425 ± 0.070 II		0.280 ± 0.006 II		0.086 ± 0.020 II	
		-1.857 ± 0.075 [c]						
		-1.838 ± 0.007 [d]						
		-1.86 ± 0.03 [e]		0.37 ± 0.09 [e]		0.268 ± 0.006 [e]		0.058 ± 0.012 [e]
				0.45 ± 0.09 [f]		0.248 [f]		0.09 ± 0.03 [f]
		-1.841 ± 0.009 [g]		0.35 ± 0.07 [g]				
						0.286 ± 0.006 [g,h]		0.058 ± 0.022 [g,h]
		-1.857 ± 0.016 [i]		0.37 ± 0.09 [i]				
						0.287 ± 0.003 [j]		0.070 ± 0.003 [j]
						0.296 ± 0.003 [k]		
^{154}Sm	-2.093 ± 0.015 I	-2.147 ± 0.047 [a]	0.540 ± 0.074 I		0.305 ± 0.006 I	0.351 [a]	0.103 ± 0.019 I	
	-2.088 ± 0.015 II	-2.053 ± 0.026 [b]	0.586 ± 0.074 II		0.299 ± 0.006 II		0.117 ± 0.019 II	
		-2.070 ± 0.012 [d]						
				0.67 ± 0.08 [f]		0.261 [f]		0.13 ± 0.03 [f]
		-2.074 ± 0.007 [g]		0.43 ± 0.08 [g]				
						0.315 ± 0.007 [g,h]		0.066 ± 0.024 [g,h]
		-2.113 ± 0.019 [i]		0.54 ± 0.11 [i]				
^{158}Gd	-2.242 ± 0.011 I	-2.302 ± 0.054 [a]	0.30 ± 0.086 I		0.332 ± 0.006 I	0.358 [a]	0.025 ± 0.021 I	
	-2.233 ± 0.011 II	-2.252 ± 0.014 [d]	0.40 ± 0.09 II		0.329 ± 0.006 II		0.049 ± 0.021 II	
		-2.23 ± 0.03 [h]		0.34 ± 0.11 [h]		0.33 ± 0.01 [h]		0.03 ± 0.025 [h]
^{160}Gd	-2.292 ± 0.014 I	-2.381 ± 0.052 [a]	$0.15^{+0.13}_{-0.15}$ I		0.349 ± 0.007 I	0.367 [a]	-0.02 ± 0.035 I	
	-2.283 ± 0.014 II	-2.29 ± 0.02 [h]	$0.28^{+0.08}_{-0.09}$ II	0.36 ± 0.10 [h]	0.337 ± 0.007 II	0.34 ± 0.01 [h]	0.016 ± 0.022 II	0.032 ± 0.024 [h]
^{164}Dy	-2.370 ± 0.020 I	-2.362 ± 0.053 [a]	$0.075^{+0.18}_{-0.28}$ I		0.349 ± 0.014 I	0.347 [a]	-0.04 ± 0.045 I	
	-2.360 ± 0.020 II	-2.36 ± 0.01 [h]	$0.25^{+0.10}_{-0.12}$ II	0.28 ± 0.11 [h]	0.337 ± 0.014 II	0.34 ± 0.01 [h]	0.005 ± 0.025 II	0.008 ± 0.029 [h]
						0.334 ± 0.005 [k]		

TABLE IV *(Continued)*

Nucleus	$M(E2;0^+\rightarrow 2^+)$	$M(E2;0^+\rightarrow 2^+)$ Other measurements	$M(E4;0^+\rightarrow 4^+)$	$M(E4;0^+\rightarrow 4^+)$ Other measurements	β_2^C	β_2^C Other measurements	β_4^C	β_4^C Other measurements
^{166}Er	-2.414 ± 0.011 I	-2.404 ± 0.042 [a]	$0.166^{+0.116}_{-0.166}$ I		0.338 ± 0.007 I	0.341 [a]	-0.017 ± 0.03 I	
	-2.404 ± 0.011 II	-2.393 ± 0.011 [d]	$0.31^{+0.09}_{-0.10}$ II		0.327 ± 0.007 II		0.017 ± 0.016 II	
		$-2.40\ \pm0.02$ [h]		$0.06^{+0.12}_{-0.18}$ [h]		$0.35\ \pm0.01$ [h]		-0.048 ± 0.04 [h]
^{168}Er	-2.454 ± 0.021 I	-2.408 ± 0.042 [a]	$0.052^{+0.17}_{-0.25}$ I		0.348 ± 0.010 I	0.339 [a]	-0.045 ± 0.04 I	
	-2.444 ± 0.021 II	-2.400 ± 0.014 [d]	$0.23^{+0.12}_{-0.15}$ II		0.335 ± 0.010 II		-0.005 ± 0.028 II	
		$-2.40\ \pm0.02$ [h]		$0.20^{+0.12}_{-0.18}$ [h]		$0.33\ \pm0.01$ [h]		-0.012 ± 0.04 [h]
						0.333 ± 0.003 [k]		
^{174}Yb	-2.448 ± 0.012 I	-2.387 ± 0.042 [a]	$0.12^{+0.17}_{-0.19}$ I		0.326 ± 0.010 I	0.317 [a]	$-0.03\ \pm0.04$ I	
	-2.438 ± 0.012 II	-2.427 ± 0.097 [c]	$0.25^{+0.13}_{-0.17}$ II		0.317 ± 0.010 II		0.002 ± 0.023 II	
		-2.418 ± 0.023 [d]						

[a] P. H. Stelson and L. Grodzins, Nucl. Data A1, 21 (1965).
[b] Reference 23.
[c] R. O. Sayer, P. H. Stelson, F. K. McGowan, W. T. Milner, and R. L. Robinson, Phys. Rev. C 1, 1525 (1970).
[d] Y. Dar, S. Kochar, and I. Tserruya, Phys. Rev. C 7, 472 (1973). The values presented in this reference are average values for many different experiments.
[e] Reference 8.
[f] Reference 10.
[g] Reference 11.
[h] Reference 12.
[i] W. Brückner *et al.*, in Proceedings of the International Conference on Nuclear Moments and Nuclear Structure, Osaka, Japan, September, 1972 (unpublished).
[j] Reference 16.
[k] Reference 31.

quantal scattering problem.[30] The interaction includes both Coulomb and nuclear parts. The long range of the Coulomb force makes it necessary to include a large number of partial waves and integrate over many nuclear radii; in order to insure convergence on the 0.1% level in all calculated cross sections in the case of ^{4}He projectiles scattered from samarium, it was necessary to include 240 partial waves and integrate to 180 fm from the center of mass.

The pure Coulomb, Coulomb plus nuclear, and pure nuclear scattering calculations, which included the 0^+, 2^+, and 4^+ states, were performed for 12 MeV incident projectiles scattering from ^{152}Sm to check nuclear-Coulomb interference near the postulated barrier, and to calculate the difference between the classical and quantal pure Coulomb calculations. The calculated nuclear-Coulomb interference effects in the 0^+, 2^+, and 4^+ cross sections of 0.06, 0.6, and 0.4%, respectively, are in agreement with the experimental results and support both the chosen "safe" bombarding energy and the contention that interference effects become significant in the 0^+ cross sections only at higher bombarding energies than in the 2^+ cross section. The optical parameters used in the calculation are those of Bruckner *et al.*[8] In addition, pure Coulomb scattering from the other nuclei was calculated for 12 MeV incident energy.

The pure Coulomb excitation calculations were compared to a three level deBoer-Winther code calculation. The quantal calculations of the 2^+ and 4^+ differential cross sections were found to be lower than the semiclassical calculations by 1.1 and 7.7%, respectively, in the case of ^{152}Sm; for ^{154}Sm the differences are 1.5 and 8.1%. The results for other nuclei are similar. These corrections fluctuate by about 0.25% as a function of center-of-mass scattering angle in 1° steps from 165 to 178°. The correction to the 2^+ cross section is therefore roughly 1% less than the correction obtained from the perturbation theory treatment of Alder *et al.*,[19] and the correction to the 4^+ cross section is 1.7% greater for ^{152}Sm, while the differences in the case of ^{154}Sm are 0.5 and 2.1%. It should be noted that the change in the calculated $P(4)$, after $M(E2; 0^+ \rightarrow 2^+)$ has been adjusted to fit the quantal $P(2)$, is almost the same for ^{152}Sm and ^{154}Sm. Since the quantal correction as obtained from the calculation of Alder *et al.*[19] varies little with bombarding energy in the energy region of interest, a second set of matrix elements $M(E2; 0^+ \rightarrow 2^+)$ and $M(E4; 0^+ \rightarrow 4^+)$ was obtained for each nucleus by correcting all the semiclassical calculations for projectile energies other than 12 MeV by the corrections calculated at 12 MeV with the code LISA. These are listed in Table IV and illustrated in Fig. 9 as Set II. It is important to note that the $P(4)$ values obtained using the perturbation theory correction differ from those obtained using the full quantal calculation by ~3% after the values of $M(E2; 0^+ \rightarrow 2^+)$ used in the calculations have been adjusted to make the calculated values of $P(2)$ agree. This is a substantial fraction of the total $E4$ contribution, especially for the nuclei ^{160}Gd to ^{174}Yb, where the change in the extracted $M(E4; 0^+ \rightarrow 4^+)$ value is 0.2 eb^2, and the final values of that matrix element are on the order of 0.1 to 0.3 eb^2.

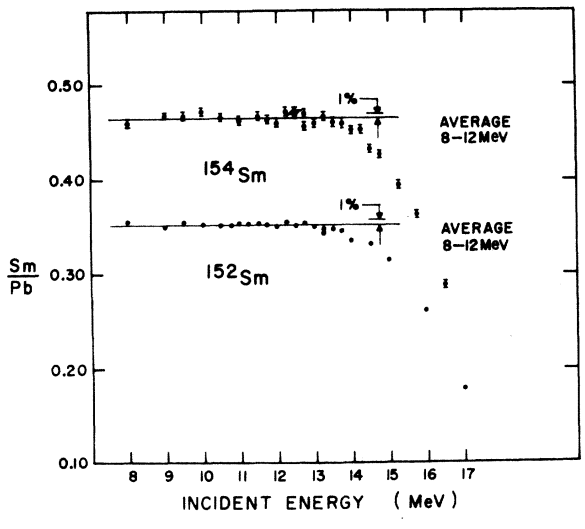

FIG. 10. Scattering from ^{152}Sm and ^{154}Sm normalized to scattering from ^{208}Pb on the same target as a function of incident ^{4}He energy. In the case of ^{152}Sm one standard deviation is indicated by the size of the points.

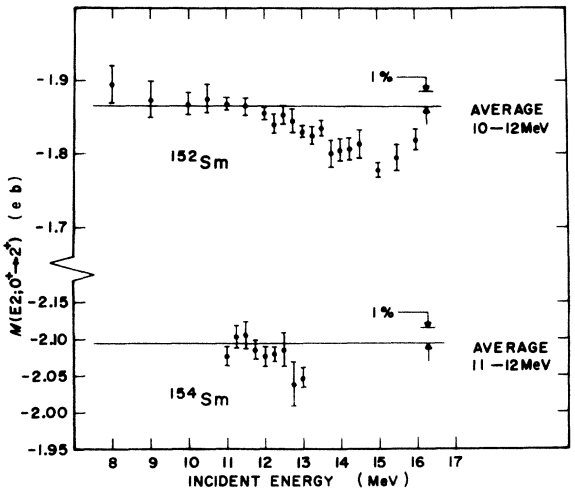

FIG. 11. Variation with ^{4}He bombarding energy of $M(E2; 0^+ \rightarrow 2^+)$ extracted under the assumption of pure Coulomb excitation of ^{152}Sm. and ^{154}Sm.

5. DISCUSSION

A. Deformation parameters

The deformation parameters, β_2 and β_4, have been extracted from the measured moments using a Fermi charge distribution with a deformed surface as suggested by the results of μ-mesic atom studies,[31] and electron scattering experiments.[16] This charge distribution is given by

$$\rho(r,\theta)=\rho_0\left[1+\exp\left(\frac{r-R(\theta)}{t}\right)\right]^{-1}, \tag{5.1}$$

$$R(\theta)=R_0[1+\beta_2 Y_2^0(\theta)+\beta_4 Y_4^0(\theta)]. \tag{5.2}$$

The moments were calculated from the deformation parameters by numerically integrating the equations

$$Q_\lambda = M(E\lambda;\,0\to\lambda) = Ze\frac{\int d\Omega \int dr\, r^{\lambda+2}\left(1+\exp\{[r-R(\theta)]/t\}\right)^{-1} Y_\lambda^0(\theta)}{\int d\Omega \int dr\, r^2\left(1+\exp\{[r-R(\theta)]/t\}\right)^{-1}}. \tag{5.3}$$

The volume and central density, ρ_0, are therefore adjusted as the deformation is changed, keeping r_0 constant at its experimentally determined value. This conserves total charge. This differs in detail from the treatment employed by some other authors,[12,17] in which the central density is kept constant at the value calculated for a spherical nucleus of the same charge and mass, as r_0 is allowed to vary with changes in deformation to keep the volume and total charge constant. It has been calculated by Bemis *et al.*[17] that the difference between these two methods (i.e., fixing r_0 and allowing ρ_0 to vary, and fixing ρ_0 and allowing r_0 to vary) changes the calculated values of ρ_0, β_2, β_4 by −1.8, −0.8, and −2.0%, respectively, for the highly deformed actinide nucleus ^{234}U ($\beta_2=0.248$, $\beta_4=0.142$). Such changes are smaller than experimental uncertainties encountered in this experiment. The results of recent electron scattering measurements performed on ^{166}Er and ^{176}Yb [32] indicate possible serious deviations from a deformed Fermi distribution with regions of enhanced density near the poles of the quadrupole shape. Such a charge density distribution would produce much larger changes in ρ_0, β_2, β_4 extracted from measured moments. The results of a typical calculation and the extraction of deformation parameters from the measured moments are shown in Fig. 12.

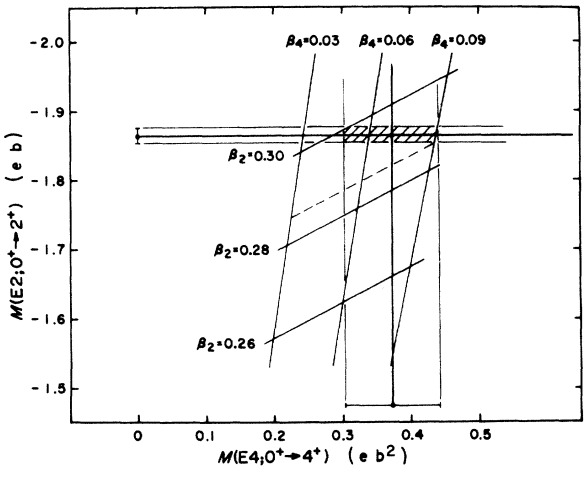

FIG. 12. Variation with β_2^C and β_4^C of $M(E2;\,0^+\to 2^+)$ and $M(E4;\,0^+\to 4^+)$ calculated from a deformed Fermi charge distribution for ^{152}Sm. The determination of β_2^C and β_4^C from the measured moments is illustrated. The errors are correlated so that both $\Delta\beta_2$ and $\Delta\beta_4$ depend mainly upon the uncertainty in $M(E4;\,0^+\to 4^+)$.

The parameters of the radial charge distribution, $r_0=R_0/A^{1/3}$ and t, were taken from the μ-mesic atom experiments,[31] which include measurements of ^{152}Sm, ^{164}Dy, and ^{168}Er. Interpolated values of these slowly varying parameters were used for the other nuclei. The extracted deformation parameters corresponding to both sets of matrix elements are shown in Table IV. It should be noted that these extracted deformation parameters are strongly dependent upon the values of r_0 and t used in the calculation. In lowest order they are expected to vary as $M(E\lambda)\propto\beta_\lambda\cdot R_0^\lambda$. As an illustration, the results of performing this analysis for the ^{152}Sm moments using three different published sets of r_0 and t are shown in Table V. When comparing determinations of β_2^C and β_4^C, caution should be exercised in order to make certain that apparent differences are not due to differences in r_0 and t used in the determination. This is, of course, especially true when comparing deformation parameters obtained from measured nuclear moments. Since the measurement of the moments themselves is free of this pitfall, a more straightforward comparison of Coulomb excitation investigations of nuclear deformation is obtained by comparing the measured moments. (It should also be remem-

TABLE V. The deformation parameters β_2^C and β_4^C extracted from the measured moments of ^{152}Sm, $M(E2;\,0^+\to 2^+)=1.865\ e$ b and $M(E4;\,0^+\to 4^+)=0.373\ e\,\text{b}^2$, using three different published sets of radial charge distribution parameters r_0 and t.

r_0	t	Reference	β_2^C	β_4^C
1.106	0.538	19	0.287	0.070
1.14	0.6	28	0.268	0.058
1.08	0.6	9	0.293	0.071

bered that, as demonstrated in Sec. 4 D, different treatments of quantal corrections to the semiclassical Coulomb excitation analysis can also produce non-trivial differences in the measured moments. The differences in the two treatments employed here yield substantial changes in the extracted moments, especially the hexadecapole moment.)

The parameters r_0 and t used in the extraction of the deformation parameters have associated with them a value of β_2 which was obtained simultaneously in the analysis of the μ-mesic atom experiment.[31] In that analysis, β_4 was assumed to be zero. If a new set of β_2, β_4 is to be substituted for that used in the μ-mesic atom experiment, it should not change the calculated values of these quantities measured in the mesic atom experiment. To check the validity of this substitution, the mean square radii of ^{152}Sm, ^{164}Dy, and ^{168}Er were calculated using both sets of β_2 and β_4 with r_0 and t being fixed in each case. The differences in the mean square radii calculated using the deformation parameters of Hitlin *et al.*[31] and those obtained in this experiment were 0.1, 0.2, and 0.3% for ^{152}Sm, ^{164}Dy, and ^{168}Er, respectively.

B. Two solutions for $M(E4; 0^+ \rightarrow 4^+)$

As was stated earlier, two different values of $M(E4; 0^+ \rightarrow 4^+)$, one positive and the other negative, can correctly predict the measured $P(4)$ for each nucleus. An examination of the β_4 deformation parameters obtained for each of the two solutions gives reasonable evidence that the positive solution is indeed the correct one. According to theory, of all the nuclei studied, ^{174}Yb should have the most negative β_4, hence the most negative $M(E4; 0^+ \rightarrow 4^+)$. This is consistent with the results of the nuclear scattering experiments. The second possible $M(E4; 0^+ \rightarrow 4^+)$ for this nucleus is ~ -0.7. This results in a β_4 of approximately -0.2. This is larger in magnitude than any predicted β_4 in the region. In addition, since the magnitude of the negative solution increases as the magnitude of the positive solution increases, it is expected that β_4 obtained from the negative solution will become more negative towards the lighter nuclei studied. This is in serious conflict with both theory and nuclear scattering results. In addition, it results in a β_4 for ^{152}Sm which is of the order of -0.25 to -0.3, and therefore is in complete disagreement with the values obtained from electron scattering measurements,[16] $\beta_4 = 0.07$.

C. Comparison of nuclear and Coulomb deformation

A comparison of Coulomb deformation parameters obtained from this experiment and nuclear deformation parameters is shown in Table VI. The variation of β_4^C with mass is shown in Fig. 13. It has been noted that these numbers are not really equivalent,[4,8,33] in part because the quantity actually extracted from the deformed optical model potential is $R_0\beta_\lambda$, where these parameters strictly refer to the optical potential distribution. As was noted in Sec. 5 A, β_λ extracted from the Coulomb excitation process depends on the radius through

TABLE VI. Comparison of Coulomb and nuclear potential deformation parameters. I and II have the same meaning as in Table IV. The entries in the "Nuclear scaled" column are the β_λ^N scaled by the ratio of charge and nuclear radii keeping the product $\beta_\lambda^N R_0$ constant; the entries in parenthesis have been scaled according to the second order corrections of D. L. Hendrie, Phys. Rev. Lett. 21, 478 (1973).

	β_2			β_4		
Nucleus	Coulomb	Nuclear	Nuclear scaled	Coulomb	Nuclear	Nuclear scaled
^{152}Sm	0.287 ± 0.006 I	0.246 [a]	0.269(0.256)	0.07 ± 0.02 I	0.048 [a]	0.052(0.061)
	0.280 ± 0.006 II	0.25 ± 0.02 [b]	0.262	0.086 ± 0.020 II	0.050 ± 0.015 [b]	0.052
		0.279 ± 0.009 [c]	0.288		0.050 ± 0.009 [c]	0.052
^{154}Sm	0.305 ± 0.006 I	0.270 [a]	0.293(0.280)	0.103 ± 0.019 I	0.054 [a]	0.059(0.071)
	0.299 ± 0.006 II	0.225 ± 0.005 [d]	0.303	0.117 ± 0.019 II	0.050 ± 0.005 [d]	0.067
		0.25 [e]	0.271		0.05 [e]	0.054
^{158}Gd	0.332 ± 0.006 I	0.282 [a]	0.306(0.295)	0.025 ± 0.021 I	0.036 [a]	0.039(0.052)
	0.329 ± 0.006 II			0.049 ± 0.021 II		
^{166}Er	0.338 ± 0.007 I	0.276 [a]	0.299(0.294)	−0.017 ± 0.03 I	0.0 [a]	0.0(0.015)
	0.327 ± 0.007 II	0.230 ± 0.005 [d]	0.310	0.017 ± 0.016 II	0.0 ± 0.005 [d]	0.0
^{174}Yb	0.326 ± 0.010 I	0.276 [a]	0.299(0.301)	−0.03 ± 0.04 I	−0.048 [a]	−0.052(−0.041)
	0.317 ± 0.010 II			0.002 ± 0.023 II		

[a] Reference 4, $r_0 = 1.2$.
[b] Reference 7, $r_0 = 1.16$.
[c] Reference 8, $r_0 = 1.14$.
[d] Reference 5, $r_0 = 1.49$.
[e] Reference 6, $r_0 = 1.2$.

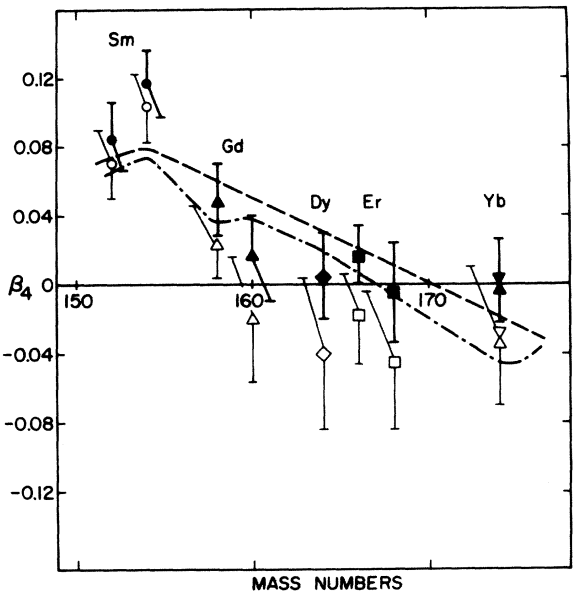

FIG. 13. β_4 as a function of mass number: The plotted points indicate the experimental β_4^C values determined in this experiment. The open symbols indicate Set I and the closed symbols indicate Set II. The dashed line indicates the trends displayed by the theoretical calculation of Ref. 1, while the dash-dot line presents the results from the calculation of Ref. 3.

$M(E\lambda) \propto \beta_\lambda R_0^\lambda$, and this radius dependence differs appreciably from the nuclear scattering case. In order to at all compare nuclear and Coulomb deformation parameters, they must be calculated under the assumption of the same nuclear radius. The third column shows β_2^N and β_4^N so scaled. Recently Hendrie[33] has considered in more detail the geometry of the scattering of α particles from the surface of a deformed nucleus, and has calculated corrections to the simple scaling by the ratio of radii. These values are shown in parenthesis for the scaled β_2^N and β_4^N values measured by Hendrie *et al.*[4]

In general, β_2^C is roughly 10% larger than β_2^N after scaling. This difference is not diminished by the second order correction. The parameters β_4^C follow roughly the same trend as β_4^N: largest and positive in the region of ^{152}Sm and ^{154}Sm, and decreasing to near zero towards the center of the rare earth region. A comparison of individual values of β_4^C and β_4^N indicates that there may exist significant discrepancies for ^{152}Sm and ^{154}Sm. Figure 8 illustrates that the Coulomb excitation measurement of $M(E4; 0^+ \rightarrow 4^+)$ or β_4^C is most reliable for nuclei with large and positive hexadecapole deformations such as ^{152}Sm and ^{154}Sm. However, it should be kept in mind that the significance of the difference between β_4^C and β_4^N found for these nuclei is subject to the considerations already discussed on the extraction of β_4 from the two types of experiments. A comparison with theoretically deduced β_4 values for the rare earth nuclei shown in Fig. 13 indicates no clear conflict, but neither is there good agreement. Similar trends have been noted in the actinide region.[17]

6. CONCLUSIONS

Inelastic scattering of ^{4}He projectiles at incident energies below the Coulomb barrier has been employed to measure the transition quadrupole and hexadecapole moments of eight even rare earth nuclei spanning the region from the transitional nucleus ^{152}Sm to ^{174}Yb, which is near the center of the group of nuclei that exhibit large static deformations. The discussion presented herein has indicated that the detection of the influence of hexadecapole excitations involves the measurement of small effects in multiple excitation of states in the ground state band, and that the accompanying high precision measurements of the excitation probabilities required can be achieved with the detection of inelastically scattered ^{4}He projectiles in a surface barrier detector. Of particular importance to the analysis of the experiments has been the determination of $M(E2; 0^+ \rightarrow 2^+)$ to about $\frac{1}{2}$% accuracy, which in some cases exceeds the accuracy of previous determinations of this matrix element by a factor of 3 to 6. Coulomb-nuclear interference effects in elastic and inelastic scattering were investigated, and it was demonstrated that Coulomb-nuclear interference occurs at a much lower energy than predicted by the simple classical formula for the Coulomb barrier, and manifests itself at different incident energies for elastic and inelastic scattering.

Static quadrupole and hexadecapole moments of the charge distribution were extracted from the measured transition matrix elements within the context of the rotational model. The additional adoption of an axially symmetric deformed Fermi shape for describing the charge distribution of these nuclei yielded charge deformation parameters, β_2^C and β_4^C, that follow the same trends as the nuclear potential deformation parameters measured in nuclear scattering experiments well above the Coulomb barrier. However, for some nuclei the Coulomb excitation β_λ values display what may be significant deviations from the nuclear potential deformations measured with the strong interaction probes. Comparisons of our measurements with other experiments employing electromagnetic interaction probes generally show good agreement. In interpreting any differences in β_4^C values derived from the latter experiments, cognizance

must be taken of the sensitivity of the derived β_4^C values to the choice of parameters such as r_0. A case in point is the discrepancy between the β_4^C value quoted by Brückner *et al.*[8] for ^{152}Sm and our value for this nucleus, which originates from differences in the r_0 values used rather than from differences in the more basic $M(E4)$ values directly measured.

Several aspects of the analysis must be understood in more detail and with higher precision than presently available if the significance of the interpretation of these data is to approach the accuracy of the primary measurements. First, the quantum mechanical problem of Coulomb scattering must be solved with a degree of accuracy which matches the current semiclassical solution, and the solution must be in a form that is as usable for routine analysis as is the deBoer-Winther code. To this end, work is currently in progress to adapt the program LISA to this purpose. This calculation will also include the effects of nuclear scattering so that the determination of the "safe" bombarding energy will be more straightforward. The successful application of this analysis to Coulomb excitation using heavier projectiles will yield more precise information on higher transition moments, moments connecting high spin states, and a more model independent measurement of $M(E4; 0^+ \rightarrow 4^+)$.

It should be noted that there exist several postulated forms of the nuclear charge distribution similar in over-all shape to the Fermi distribution used in this analysis.[16,17] Since these involve more parameters than the Fermi distribution, there is as yet no strong evidence as to whether they provide a more realistic representation of the charge distribution. Further studies by means such as electron scattering could provide this type of information.

It is clear that in order to consolidate the information derived from both electromagnetic and strong interaction probes, it is necessary to develop a unique correspondence between the deformations described by β_λ^C and β_λ^N and a method of relating the charge distribution and the nuclear potential distribution to the nuclear mass distribution. Until a relationship is firmly established between Coulomb deformation as, for example, parametrized by a deformed Fermi charge distribution, and the nuclear potential deformation described by the parameters of a deformed optical potential, these two descriptions of nuclear deformation should be viewed as complementary information and not necessarily as measurements of the same thing.

7. ACKNOWLEDGMENTS

The authors would like to thank Professor D. Allan Bromley for many interesting and helpful discussions and for his continuing interest in the work. We gratefully acknowledge the aid of Mr. K. Sato and the operating staff of the MP1 accelerator for diligently providing the ^{4}He beams, Dr. E. B. Fehr for aid and instruction in fabricating the targets, and Mr. C. E. L. Gingell for assistance with the instrumentation. In addition, we would like to thank Dr. C. K. Davis and Mr. Richard Hadsell for their assistance in obtaining the data, and Dr. R. J. Ascuitto for the use of his scattering code LISA and his extensive efforts in adapting it to perform the high precision Coulomb excitation calculation.

---

*Work supported under U. S. Atomic Energy Commission Contract No. AT(11-1)-3074.

[1]P. Möller, B. Nilsson, S. G. Nilsson, A. Sobiczewski, Z. Szymanski, and S. Wycech, Phys. Lett. 26B, 418 (1968).

[2]S. G. Nilsson, C. F. Tsang, A. Sobiczewski, Z. Szymanski, S. Wycech, C. Gustafson, I. Lamm, P. Möller, and B. Nilsson, Nucl. Phys. A131, 1 (1969).

[3]U. Götz, H. C. Pauli, K. Alder, and K, Junker, Nucl. Phys. A192, 1 (1972).

[4]D. L. Hendrie, N. K. Glendenning, B. G. Harvey, O. N. Jarvis, H. H. Duhm, J. Saudinos, and J. Mahoney, Phys. Lett. 26B, 127 (1968).

[5]A. A. Aponick, C. M. Chesterfield, D. A. Bromley, and N. K. Glendenning, Nucl. Phys. A159, 367 (1970).

[6]P. H. Brown and P. Stoler, Phys. Rev. C 2, 765 (1970).

[7]M. P. Barbier, R. M. Lombard, J. M. Moss, and Y. D. Terrien, Phys. Lett. 34B, 386 (1971).

[8]W. Bruckner, J. G. Merdinger, D. Pelte, U. Smilansky, and K. Traxel, Phys. Rev. Lett. 30, 57 (1973).

[9]A. Winther and J. deBoer, in *Coulomb Excitation*, edited by K. Alder and A. Winther (Academic, New York, 1966).

[10]F. S. Stephens, R. M. Diamond, N. K. Glendenning, and J. deBoer, Phys. Rev. Lett. 24, 1137 (1970); F. S. Stephens, R. M. Diamond, and J. deBoer, Phys. Rev. Lett. 27, 1151 (1971).

[11]T. K. Saylor, III, J. X. Saladin, I. Y. Lee, and K. A. Erb, Phys. Lett. 42B, 51 (1972).

[12]K. A. Erb, J. E. Holden, I. Y. Lee, J. X. Saladin, and T. K. Saylor, Phys. Rev. Lett. 29, 1010 (1972).

[13]W. Ebert, P. Hecking, K. Pelz, S. G. Steadman, and P. Winkler, Z. Phys. 263, 191 (1973).

[14]J. S. Greenberg and A. H. Shaw, J. Phys. Soc. Jap. Suppl., 34, 362 (1973).

[15]P. Winkler, Nucl. Phys. A168, 139 (1971).

[16]W. Bertozzi, T. Cooper, N. Ensslin, J. Heisenberg, S. Kowalski, M. Mills, W. Turchinetz, C. Williamson,

S. P. Fivozinsky, J. W. Lightbody, Jr., and S. Penner, Phys. Rev. Lett. 28, 1711 (1972).
[17]C. E. Bemis, Jr., F. K. McGowan, J. L. C. Ford, Jr., W. T. Milner, P. H. Stelson, and R. L. Robinson, Phys. Rev. C 8, 1466 (1973).
[18]Z. Berant, R. A. Eisenstein, J. S. Greenberg, Y. Hurowitz, U. Smilansky, and P. N. Tandon, Phys. Rev. Lett. 27, 110 (1971); Nucl. Phys. A196, 312 (1972).
[19]K. Alder, F. Roesel, and R. Morf, Nucl. Phys. A186, 449 (1972).
[20]I. A. Fraser, J. S. Greenberg, S. H. Sie, R. G. Stokstad, G. A. Burginyon, and D. A. Bromley, Phys. Rev. Lett. 23, 1047 (1969).
[21]I. A. Fraser, J. S. Greenberg, S. H. Sie, R. G. Stokstad, and D. A. Bromley, Phys. Rev. Lett. 23, 1051 (1969).
[22]R. G. Stokstad, J. S. Greenberg, I. A. Fraser, S. H. Sie, and D. A. Bromley, Phys. Rev. Lett. 27, 748 (1971).
[23]R. M. Diamond, F. S. Stephens, K. Nakai, and R. Nordhagen, Phys. Rev. C 3, 344 (1971); R. M. Diamond, G. D. Symons, J. Quebert, H. Maier, J. Leigh, and F. S. Stephens, Nucl. Phys. A184, 481 (1972).
[24]K. Alder, R. Morf, and F. Roesel, Phys. Lett. 32B, 645 (1970).
[25]R. J. Ascuitto, code LISA, private communication.
[26]G. D. Symons and A. C. Douglas, Phys. Lett. 24B, 11 (1967).
[27]J. X. Saladin, J. E. Glenn, and R. J. Pryor, Phys. Rev. 186, 1248 (1969).
[28]L. I. Foldy and E. Eriksen, Phys. Rev. 95, 1048 (1954).
[29]R. H. Stelson, C. E. Bemis, Jr., F. K. McGowan, W. T. Milner, J. C. L. Ford, Jr., R. L. Robinson, and W. Tuttle, in *Proceedings of the International Conference on Nuclear Physics, Munich, 1973*, edited by J. de Boer and H. J. Mang (North-Holland, Amsterdam/American Elsevier, New York, 1973), Vol. 1, p. 371.
[30]N. K. Glendenning, in *Nuclear Structure and Nuclear Reactions, Proceedings of the International School of Physics, "Enrico Fermi," Course 40*, edited by M. Jean and R. A. Ricci (Academic, New York, 1967).
[31]D. Hitlin, S. Bernow, S. Devons, I. Duerdoth, J. W. Kast, E. R. Macagno, J. Rainwater, C. S. Wu, and R. C. Barrett, Phys. Rev. C 1, 1184 (1972).
[32]J. Heisenberg *et al.*, in *Proceedings of the International Conference on Nuclear Physics, Munich, September, 1973* (see Ref. 29), Vol. 1, p. 629.
[33]D. L. Hendrie, Phys. Rev. Lett. 21, 478 (1973).